Influence of Al2O3 addition on structure and mechanical properties of borosilicate glasses

Sebastian Bruns, Tobias Uesbeck, Dominik Weil, Doris Möncke, Leo van Wüllen, Karsten Durst, Dominique de Ligny

Angaben zur Veröffentlichung / Publication details:

Bruns, Sebastian, Tobias Uesbeck, Dominik Weil, Doris Möncke, Leo van Wüllen, Karsten Durst, and Dominique de Ligny. 2020. "Influence of Al2O3 addition on structure and mechanical properties of borosilicate glasses." *Frontiers in Materials* 7 (July): 189. https://doi.org/10.3389/fmats.2020.00189.

frontiers in Materials

ORIGINAL RESEARCH
published: 28 July 2020
doi: 10.3389/fmats.2020.00189

Influence of Al_2O_3 Addition on Structure and Mechanical Properties of Borosilicate Glasses

Sebastian Bruns[1], Tobias Uesbeck[2,3]*, Dominik Weil[1], Doris Möncke[4], Leo van Wüllen[3], Karsten Durst[1] and Dominique de Ligny[2]*

[1] Physical Metallurgy, Technical University Darmstadt, Darmstadt, Germany, [2] Institute of Glass and Ceramics, Friedrich-Alexander-University Erlangen-Nürnberg, Erlangen, Germany, [3] Institute of Physics, Augsburg University, Augsburg, Germany, [4] Inamori School of Engineering at the New York State College of Ceramics, Alfred University, Alfred, NY, United States

Alkali-borosilicate glasses are one of the most used types of glasses with a high technological importance. In order to optimize glasses for diverse applications, an understanding of the correlation between microscopic structure and macroscopic properties is of central interest in materials science. It has been found that the crack initiation in borosilicate glasses can be influenced by changes in network interconnectivity. In the NBS2 borosilicate glass system ($74.0SiO_2$-$20.7B_2O_3$-$4.3Na_2O$-$1.0Al_2O_3$ in mol%) two subnetworks are present, i.e., a silicate and a borate network. Increasing cooling rates during processing were found to improve glasses crack resistance. Simultaneously, an increase in the network interconnectivity accompanied by an increasing capacity for densification were noticed. Their individual contribution to the mechanic response, however, remained unclear. In the present study the borosilicate glasses were systematically modified by addition of up to 4.0 mol% Al_2O_3. Changes in the network connectivity as well as the short- and medium-range order were characterized using Raman and NMR spectroscopy. Both the Raman and the ^{11}B NMR results show that four-fold-coordinated boron is converted into three-fold-coordination as the Al_2O_3 content increases. Additionally, ^{27}Al NMR experiments show that aluminum is dominantly present in four-fold coordination. Aluminum-tetrahedra are thus charge balanced by sodium ions and incorporated into the silicate network. Finally, nanoindentation testing was employed to link the inherent glass structure and its network configuration to the mechanical glass response. It was found that the glass softens with increasing Al_2O_3 content, which enhances the crack resistance of the borosilicate glass.

Keywords: spectroscopy, Raman, Brillouin, NMR, mechanical testing, glass structure, indentation

OPEN ACCESS

Edited by:
Lothar Wondraczek, Friedrich Schiller University Jena, Germany

Reviewed by:
Satoshi Yoshida, Asahi Glass, Japan
Morten M. Smedskjaer, Aalborg University, Denmark

****Correspondence:***
Sebastian Bruns
s.bruns@phm.tu-darmstadt.de
Tobias Uesbeck
tobias.uesbeck@physik.uni-augsburg.de

Specialty section:
This article was submitted to Ceramics and Glass, a section of the journal Frontiers in Materials

Received: *10 January 2020*
Accepted: *22 May 2020*
Published: *28 July 2020*

Citation:
Bruns S, Uesbeck T, Weil D, Möncke D, van Wüllen L, Durst K and de Ligny D (2020) Influence of Al_2O_3 Addition on Structure and Mechanical Properties of Borosilicate Glasses. Front. Mater. 7:189. doi: 10.3389/fmats.2020.00189

INTRODUCTION

Nowadays oxide glasses are important structural and functional components. The variety of possible applications places different demands on the material. While glass fibers are intended to be stiff, glass used for protective screens needs to be rather flexible (Gross and Price, 2017; Januchta et al., 2019b). The reliability of glass, however, is usually limited by brittle fracture. Approaches to design damage resistant glass are of high scientific significance (Wondraczek et al., 2011); ranging

from local ion implantation (Price et al., 2009; Gross and Price, 2017) over compositional design (Malchow et al., 2015; Rosales-Sosa et al., 2016; Januchta et al., 2019b) to changes in the thermal history (Malchow et al., 2015; Zehnder et al., 2017a). Multi-component alkali-borosilicate glasses represent a widely used type of special glasses with a high technological importance. Low alkali glasses, for instance, exhibit a low thermal expansion coefficient and a relatively high softening temperature. They are highly resistant against thermal shock, chemically resistant, and exhibit a high hardness as well as good optical properties. This makes them suitable for a wide range of applications, such as for substrates in electronic devices or as household and laboratory ware (Ellison and Cornejo, 2010; Mauro, 2014; Smedskjaer et al., 2014). They are used for toxic and nuclear waste immobilization but also in high performance optics (Ehrt, 2000; Rouxel, 2007). A general understanding of the correlation between the network structure and the mechanical response is essential to tailor enhanced properties in multi-component alkali poor borosilicate glasses (Kurkjian et al., 2010; Wondraczek et al., 2011; Mauro, 2014).

Glass processing (thermal history and pressure) and chemical alterations can strongly influence the structure in boron-containing glasses. In this context, the coordination of boron can change from three-fold BO_3 (B^{III}) to four-fold $[BO_4]^-$ (B^{IV}) units. Thereby, differences in the structural homogeneity of the glass are introduced (Dell et al., 1983; Möncke et al., 2003, 2006; Wondraczek et al., 2007, 2010). The network structure of borosilicate glass can be investigated based on experimental ^{11}B NMR results (Dell et al., 1983; Wondraczek et al., 2007). The model by Dell and Bray (Yun and Bray, 1978; Yun et al., 1979; Dell et al., 1983) describes the mechanism behind the creation of non-bridging oxygen atoms (nbO) and thereby the structural evolution of the glass when alkali cations are added. The values of R and K, defined as $[Na_2O]/[B_2O_3]$ and $[Si_2O]/[B_2O_3]$, are especially helpful for predicting structural changes with chemical variation. Nevertheless, it has to be considered that the model of Bray and Dell exhibits some limitations. The model predicts complete phase separation for binary borosilicate glasses, whereas Wang and Stebbins (1998) and Martens and Müller-Warmuth (2000) were able to show that there is a considerable mixing of B_2O_3 and SiO_2 networks. With increasing amount of modifier oxides, neutral trigonal BO_3-units are transformed into charged $[BO_4]^-$ units. Thereby, planar units (B^{III}) are transformed into tetrahedral units (B^{IV}) reinforcing the three-dimensionality of the glass network. As a consequence, the network structure is strengthened (Biscoe and Warren, 1938; Vogel, 1994). In contrast to silica glass, where the network depolymerizes continuously as the network modifier content increases (and the share of nbO increases), borosilicate glasses behave differently. The network connectivity in borosilicate glasses initially increases, which strengthens the glass. At a certain point, when R reaches a value of 0.5, the behavior changes and a further increase of the modifier oxide concentration leads to the formation of nbO on trigonal borate and/or silicate tetrahedra (Milberg et al., 1972; Möncke et al., 2003; Winterstein-Beckmann et al., 2014a). In low-R glasses, where R is smaller than 0.5, the fraction of four coordinated boron N_4 can be approximated to equal to R (Möncke et al., 2003; Winterstein-Beckmann et al., 2013; Januchta et al., 2019b). In this range the *R*-value of 0.2 defines the line of boron oxide anomaly at which many material properties exhibit extrema (Möncke et al., 2003; Winterstein-Beckmann et al., 2014a). Those features make borosilicate glasses a very interesting system to study the link between structural alterations to the mechanical response (Winterstein-Beckmann et al., 2014a,b; Malchow et al., 2015; Zehnder et al., 2017a,b).

Instrumented (nano-)indentation testing has become a widely used tool to investigate the deformation mechanisms of glass, as it activates a variety of possible responses: elastic contact, inelastic shear flow, densification and cracking (Rouxel, 2015; Yoshida et al., 2016; Januchta and Smedskjaer, 2019; Yoshida, 2019). Whereas, indentation-based methods to asses fracture toughness and their applicability to oxide glasses is controversially discussed in the literature (Bruns et al., 2017, 2020; Rouxel and Yoshida, 2017; Yoshida, 2019), indentation testing remains one of the best solutions to compare glasses in terms of critical loads for crack initiation (Wada et al., 1974; Kato et al., 2010; Yoshida, 2019). Significant shifts in crack resistance have been observed upon chemical variations (Kato et al., 2010; Barlet et al., 2015; Malchow et al., 2015), different thermal histories (Malchow et al., 2015; Zehnder et al., 2017a), or upon compression (Januchta et al., 2017). Enhanced crack initiation loads were often referred to excess free volume and enhanced densification contribution to the deformation process (Kato et al., 2010; Januchta et al., 2017; Yoshida, 2019).

The sodium borosilicate glass NBS2 exhibits a composition (74 SiO_2-20.7 B_2O_3-4.3 Na_2O-1.0 Al_2O_3 mol%) which places the glass directly on the line of the boron oxide anomaly (Möncke et al., 2006). The glass exhibits some interesting features, i.e., that the network structure can be influenced by the thermal history of the glass (Möncke et al., 2003, 2006, 2015b). Small pieces of quenched NBS2 exhibits superior fracture properties, which have been attributed to changed subnet connectivity and the larger extent of free volume (Malchow et al., 2015). Quenching, however, limits both sample size and reproducibility. In general, quenching suppresses phase separation by freezing the high temperature configuration of the glass (Möncke et al., 2003, 2006, 2015b). Al_2O_3 can be added for a similar purpose to the sodium borosilicate glass, namely to overpass the miscibility gap (Möncke et al., 2003).

In the present study, a larger fraction of Al_2O_3 is added to the NBS2 glass composition. The effect of Al_2O_3 addition on the network structure and the mechanical response is investigated and compared to quenching effects. Elastic-plastic properties from indentation testing and Brillouin spectroscopy are correlated to short- and midrange structural changes measured by Raman and $^{11}B/^{27}Al$ solid-state NMR. Finally, the fracture behavior is investigated using high load nanoindentation.

EXPERIMENTAL PROCEDURES

Glass Melting/Preparation

NBS2 borosilicate glasses with increasing Al_2O_3 content were prepared in 50 g batches using standard melt cooling methods.

The NBS ratio (74 SiO_2-20.7 B_2O_3-4.3 Na_2O mol%) was kept constant while the Al_2O_3 content was successively increased from 1.0 to 4.0 mol%. The starting materials SiO_2 (Sigma Aldrich, 99% p.a.), H_3BO_3 (Roth, ≥99.8%), Na_2CO_3 (Sigma Aldrich ≥99.5%) and Al_2O_3 (Sigma Aldrich) were mixed and dried for approximately 12 h at 400°C in a covered platinum-rhodium crucible. Glass melting was performed in a platinum crucible at 1,100°C (heating rate of ∼20 K/min) with a dwell time of 30 min in order to evaporate CO_2. In the next step the temperature was increased to 1,500°C with a heating rate of ∼10 K/min. The temperature was kept constant for 60 min with a closed lid to avoid possible evaporation. After this step the temperature was increased to 1,600°C and held constant for another 45 min. Just before pouring the glass onto a brass block the furnace was raised to 1,650°C to improve the flow properties. Finally, the samples were crushed and molten one more time to ensure a homogeneous mixture. During cooling the melt was first poured into a preheated graphite mold (500°C) which was slowly cooled down to room temperature with a cooling rate of about 30 K/h. These samples are referred to as "furnace cooled" (fc). Additionally, samples of each composition were fast cooled by quenching in water, in the order of 200°C/s, hence they are referred to as "quenched" (qu). The henceforth discussion refers to the "furnace cooled" condition if the cooling rate is not specified. The sample containing 4.0 mol% Al_2O_3 was too viscous to pour, so the melt was transferred with the crucible in the preheated furnace and cooled down to room temperature. Subsequently the sample was drilled out of the crucible.

Densities were measured by the Archimedes method in toluene. At least 5 pieces between 0.1 and 1.0 g of weight were used and the mean and standard deviation of the results are given in **Table 3**. ICP-OES (Inductively Coupled Plasma—Optical Emission Spectrometry) was performed to analyze the chemical composition. **Table 1** summarizes the glass compositions. It is shown that the determined proportion of B_2O_3 is ∼5 mol% higher than the intended weighed amount. Simultaneously the SiO_2 content is also ∼5 mol% lower than intended. A typical error source for quantitative analysis by ICP-OES is incomplete dissolution of borosilicate glasses, where silica is known to be easily be underrepresented in solution. Unfortunately, the light element boron is hard to quantify with SEM-EDX (Scanning Electron Microscope—Energy Dispersive X-ray Spectroscopy) or XRF (X-ray Fluorescence Spectroscopy). The negligible loss of volatile boron from the melt was however confirmed by the measured B/Al-ratio, which was close to the expected values. A systematic, near constant loss of sodium ions during melting is however revealed by quantitative analysis. Since the sodium concentration remains constant, the discussion of the competing efforts of aluminate and borate units for the modifier oxide on structure and properties is not affected by the deviation from the nominal composition. Since effects of Al_2O_3 addition are of prime interest in the present study the samples are labeled according to their Al_2O_3 content. The nominal compositions were used in the manuscript henceforth in order to keep labeling simple.

Nanoindentation Testing

Nanoindentation testing was performed using a Keysight[1] G200 nanoindenter. The indentation tests were executed under air-conditioned laboratory conditions (humidity in the range of 33%) at room temperature using a Synton-MDP[2] Berkovich pyramidal indenter as default tip geometry. Tip area function and machine compliance were calibrated on a commercial fused silica reference sample according to the procedure of Oliver and Pharr (1992). Indentation testing was performed in continuous stiffness mode (CSM) a constant strain rate $\dot{\varepsilon}$ of 0.05 s^{-1}. In CSM mode the loading cycle is superimposed with a 2 nm amplitude displacement oscillation at 45 Hz, which allows to record hardness H and indentation modulus E_I as a function of penetration depth. Hardness and modulus values were averaged in a depth range between 500 and 2,000 nm using at least 9 performed indentations. In this depth range, both hardness and modulus exhibit a depth independent, constant value.

Indentation fracture was studied in high load mode with a default step size of 1 N and a maximum loading of 10 N using a constant loading rate of 0.1 N/s. This study also included sharper three-sided pyramidal tips having centerline-to-face angles of 50° and 35.26° (Cube Corner) as well as a four-sided Vickers pyramid.

Solid State NMR

Single resonance MAS-NMR (Magic Angle Spinning—Nuclear Magnetic Resonance) spectra were recorded at 7.0 and 11.7 T using a Bruker Avance III 300 MHz spectrometer and a Varian VNMRs 500 NMR spectrometer. Single pulse ^{27}Al and ^{11}B spectra were measured in commercial MAS-NMR probes using 4 mm and 1.6 mm rotors. The operation conditions are specified in **Supplementary Table 1**. Chemical shifts are reported relative to an aqueous solution of 1 M $Al(NO_3)_3$ ($\delta_{iso} = 0$ ppm) and a 1 M H_3BO_3 solution ($\delta_{iso} = 0$ ppm). ^{11}B triple-quantum (TQ)-MAS-NMR spectra were measured at 11.7 T at a spinning speed of 25.0 kHz using the three-pulse zero-filtering sequence (Medek et al., 1995). The hard excitation and reconversion pulses were 1.0 and 4.0 μs long. The third soft detection pulse had a duration of 10 μs and the relaxation delay was 5 s. The program DMFit was used to analyze the spectra (Massiot et al., 2002).

Raman/Brillouin

Polished glass plates (co-planar for platelet Brillouin) were used for Raman and Brillouin spectroscopic studies. Raman spectra were obtained in the range from 100 to 1,600 cm^{-1} with a Thermo Nicolet Almega XR Raman using a 532 nm laser excitation. To achieve a good spectral resolution each spectrum was collected with 5 scans of 120 s exposure time with a 50x objective. The spectra were background corrected with a polynomial function and normalized to the total area using the LabSpec® software by HORIBA Scientific.

Brillouin spectra in backscattering (180°) and platelet (45°) geometries were measured with an Associated Raman Brillouin Calorimetry (ARABICA) set up (Veber et al., 2017). The samples

[1]Keysight Technologies, Inc., Santa Rosa, CA, United States.
[2]Synton-MDP AG, Nidau, Switzerland.

TABLE 1 | Nominal and measured compositions of the glasses under investigation.

Glass	SiO_2 [mol%]		B_2O_3 [mol%]		Na_2O[mol%]		Al_2O_3 [mol%]	
	Nominal	ICP-OES	Nominal	ICP-OES	Nominal	ICP-OES	Nominal	ICP-OES
1.0% Al	74.00	69.75	20.70	25.59	4.30	3.32	1.00	1.33
1.5% Al	73.62	68.34	20.60	26.35	4.28	3.47	1.50	1.82
2.0% Al	73.25	68.60	20.49	25.77	4.26	3.34	2.00	2.28
4.0% Al	71.76	68.22	20.07	24.57	4.17	3.40	4.00	3.81

were excited with a 488 nm laser with 100 mW. The mean of the Anti-Stokes and the Stokes peak positions were used. For the platelet measurements, polished and coplanar thin samples were measured under a 45° angle. The Poisson's ratio (ν) can be directly calculated from the ratio between the longitudinal and transversal mode peak positions. For the backscattered measurements the laser beam was focused with a microscope (50x objective) at roughly 10 μm below the surface. The refractive index n was measured at 488 nm using an Abbé refractometer. From the backscattering measurement and using the sample refractive index and density the longitudinal modulus M was estimated. Then all the other elastic moduli: Young's (E), Shear (G), and Bulk (K) can be determined (Polian, 2003; Reibstein et al., 2011). Coupling the two geometries reduce very significantly the uncertainties which were evaluated by error propagation.

RESULTS

The Effect of Al_2O_3 Addition on the Glass Structure

Structural changes in the NBS2 borosilicate glass upon Al_2O_3 addition were studied using both NMR and Raman spectroscopy. Alterations of the Raman spectra with increasing Al_2O_3 amount are shown in **Figure 1** for the "furnace cooled" series.

Raman Spectroscopy

Four dominant regions which can be associated with structural changes can be distinguished in the Raman spectra. The small shift to higher wave numbers with increasing Al_2O_3 amount in the silicate network deformation mode (200–620 cm^{-1}) can be associated with a change of the ring size in the silicate sub-network or a small decrease of the mean angle between tetrahedra. The small band at about 600 cm^{-1} increases slightly with increasing Al_2O_3 content, which indicates the presence of three membered silicate rings. The region between 700 and 850 cm^{-1} shows the typical breathings modes for boroxol (805 cm^{-1}) and borate rings with one or two four-fold coordinated boron units (∼770 and 760 cm^{-1}). As observed in **Figure 1C** the boroxol ring band increases with increasing Al_2O_3 amount whereas the amount of four-fold coordinated boron decreases and finally vanishes for the sample with 4.0 mol% Al_2O_3. This indicates that sodium favors aluminum instead of boron for charge compensation. Hence, Al takes the role of an additional network former in the glasses.

The stretching vibrations of the Si-O (in fully polymerized Q^4 units, silicate tetrahedra with 4 bridging oxygen atoms) and mixed Si-O-B bonds can be seen in the region between 950 and 1,250 cm^{-1} (**Figure 1D**).

All modes intensities increase with increasing Al_2O_3 content, while the intensity of the high energy side of Q^4 modes increases faster than the lower energy bands of the same Si-O stretching envelop-modes. The observed variations might reflect a change of connectivity from Si-O-B^{III} to Si-O-Al^{IV}. In the region of highest frequency (between 1,250 and 1,600 cm^{-1}) no significant changes with Al variation can be observed. B^{III}-O stretching modes of rings are weaker in relative intensity than the ring breathing modes observed at 750–800 cm^{-1} and the small variations of ring B^{III}-O vs. non-ring B^{III}-O populations upon Al_2O_3 addition (see NMR section here below) do not result in significant changes of the high frequency envelop.

NMR Spectroscopy

NMR spectroscopy can be used to study the local environments of individual elements and helps in the unambiguous assignment of Raman bands and thus the verification of the Raman results. **Figure 2** shows the ^{27}Al MAS-NMR spectra (Magic Angle Spinning) of the furnace cooled series. Only the central transition of the ^{27}Al nuclear spins ($I = 5/2$) is observed in these spectra. The spectra show the typical asymmetric line shapes which are centered at around 45 ppm. This suggests that most of the Al is four-fold coordinated while the relative broad line shapes can be explained by a broad distribution of the existing quadrupole parameters. These findings correspond well to observations on charge balanced sodium aluminosilicate glasses in the literature (Eckert, 1992, 1994; Eden, 2015). For the investigated glasses, the chemical shift indicates that aluminum must be fully present as negatively charged $[AlO_4]^-$ units. The $[AlO_4]^-$ is charge balanced by positive charged sodium ions in order to achieve charge neutrality in the glass. Thus, Al is completely incorporated into the polymerized glass network.

The effect of Al_2O_3 addition on the ^{11}B MAS-NMR spectra is shown in **Figure 3A**. The spectra (solid lines) can generally be deconvoluted into two distinct types of line shape components. One belongs to four-fold coordinated boron (B^{IV}, Gaussian line near 0 ppm) and the broader one is correlated to three-fold coordinated boron (two anisotropic line shapes between δ_{iso} = 17 and 13 ppm) arising from interactions of the nuclear electric quadrupole moment of the ^{11}B with electrostatic field gradients created by the trigonal planar bonding geometry of three-coordinate boron (B^{III}) species. Due to the different

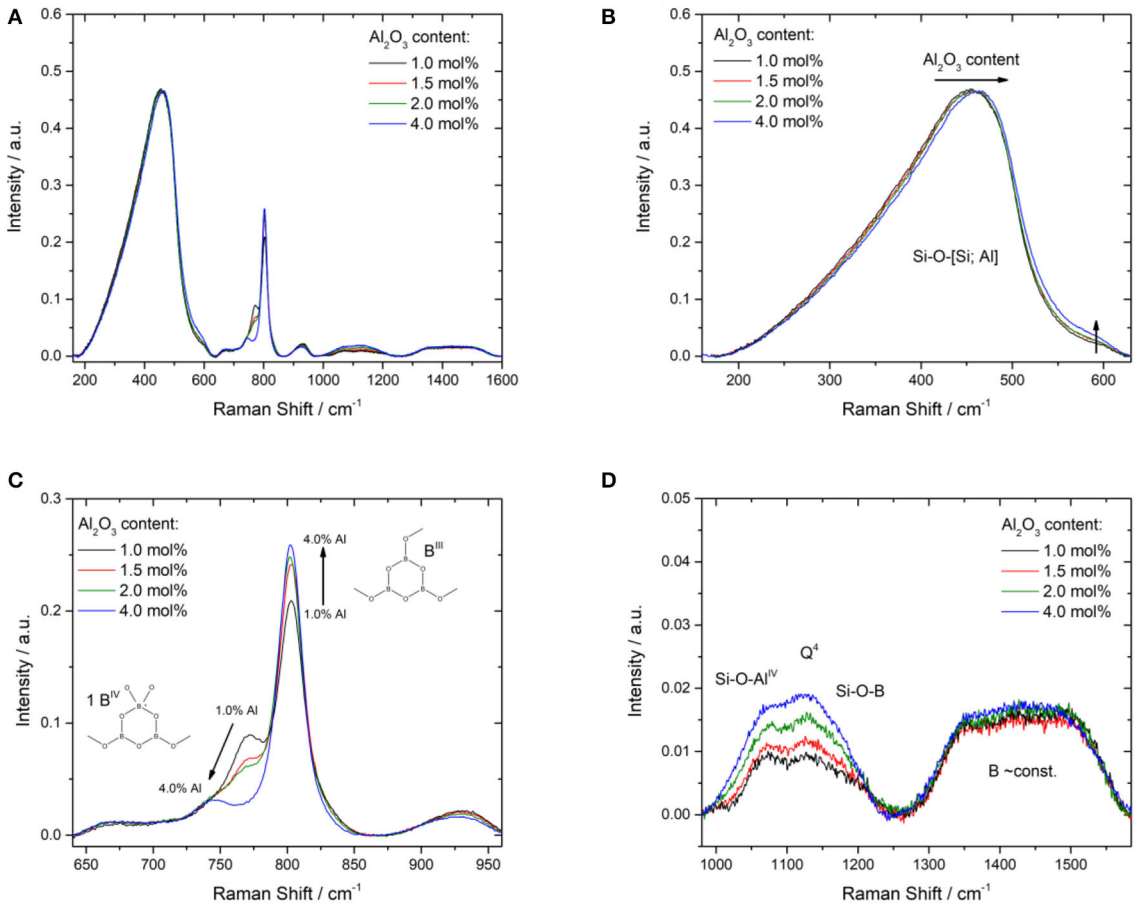

FIGURE 1 | (A) Area normalized Raman spectra of NBS2 glasses with changing Al_2O_3 amount. Enlarged details show the silicate deformation modes **(B)** between 150 and 650 cm^{-1}, the borate and boroxol ring modes **(C)** between 675 and 850 cm^{-1}, and **(D)** stretching modes of borate tetrahedra at 920 cm^{-1}, Si-O stretching modes between 950 and 1,250 cm^{-1}, and of trigonal borate entities between 1,250 and 1,600 cm^{-1}.

environment, the broad resonance in the range 18–2 ppm can be divided into two signal components typical for boron. The broad signal consists of two signal components with a characteristic line shape for the central m = ½ <-> m = −½ transition of a spin-3/2 ^{11}B nuclear isotopes that can be assigned to the B^{III}. Martens et al. assigned in binary borosilicate glasses the signal near 17 ppm to boroxol rings. They assigned the signal near 13 ppm, found in high silicate borosilicate glasses, to boron atoms in mixed borosilicate phase (Martens and Müller-Warmuth, 2000). van Wüllen and Schwering (2002) extended this model and assigned the signal close to 17 ppm to boroxol rings in a borate-like network and the signal near 13 ppm as a superposition of B^{III} units in a borate environment and B^{III} units in a borosilicate environment. Previous studies on this glass system were also able to prove a spatial proximity of the B^{III} and B^{IV} to Si by 2D $^{11}B/^{29}Si$ correlation experiments (Du and Stebbins, 2003; Möncke et al., 2015a). In the literature, a chemical shift of about 0 ppm for the B^{IV}-units is attributed to tetrahedral borate units where one B-atom is connected to 3 silica and 1 boron group. A quantitative deconvolution of the line shape allows to determine the fraction of both boron species (MacKenzie and Smith, 2002). All line shape parameters used for fitting the spectra are listed in **Supplementary Table 2**. For the glass with the lowest Al_2O_3 content the highest fraction of B^{IV} at 12% is measured. With increasing Al content, the amount of B^{IV} decreases (**Figure 3B**).

For the three-coordinated boron species the low value of the electric field gradient asymmetry parameter (0.25 ± 0.03) indicates a species close to axial symmetry such as the one known for neutral trigonal coordinated boron, B^{III}. As expected from the composition, anionic meta- or pyroborate groups for which asymmetry parameters close to 0.5 are expected (Stebbins et al., 2000) can be ruled out since their typical line shapes are not visible in the recorded spectrum. A closer look at the data indicates that there are two distinct types of B^{III} species present in the MAS-NMR spectra, showing different chemical shifts. A ^{11}B-MQMAS (Multi Quantum MAS) experiment was performed on one sample (2.0 mol% Al_2O_3) in order to verify this observation. The MQMAS allows to resolve the previously overlapping signals into two isolated line shapes by selective investigation of the multi quantum transitions (here triple quantum). A representative

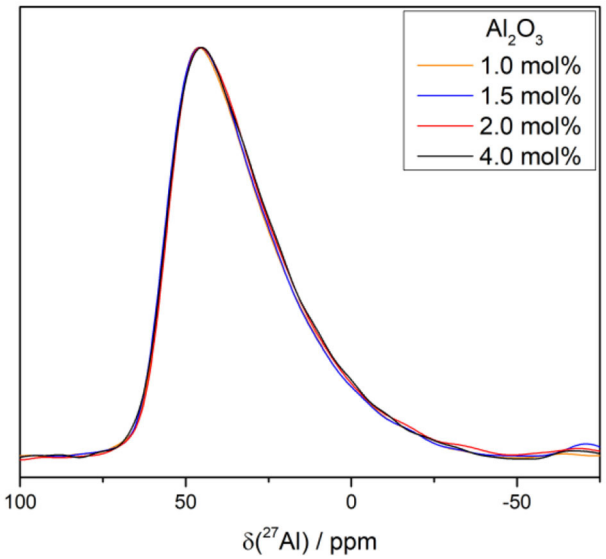

FIGURE 2 | ^{27}Al MAS-NMR spectra of the furnace cooled NBS2-Glasses at 300 MHz.

deconvolution is shown in **Figure 3A** (dotted lines) and for a typical ^{11}B-MQMAS as presented in **Figure 3C**. The dominant species near 17 ppm can be characterized with B^{III} units showing connectivity with other boron species whereas the B^{III} groups close to 13 ppm indicate B^{III} units taking part in non-ring structures like B-O-Si linkages (Möncke et al., 2015b).

The deconvolution results from the NMR investigation are summarized in **Figure 3B** and **Supplementary Data**. The original Dell and Bray model (R) (Dell et al., 1983) does not consider the incorporation of Al_2O_3 in the glass structure. For our compositions since K is 3.6, R-values express directly N_4 and remain constant at 0.21, showing that there should be no change in boron coordination. The NMR results disprove this simplification. If now the sodium fraction mobilized to compensate the aluminum is taken into account, a modified fraction of four-coordinated boron R' can be evaluated according to Januchta et al. (2019b).

$$R' = N_{4Charge\ compensation} = \frac{[Na_2O] - [Al_2O_3]}{[B_2O_3]} \quad (1)$$

Here it is evident that the proportion of B_4 decreases with increasing amount of Al whereas the share of B^{III} increases (**Table 2**). This view agrees well with the ^{11}B-NMR results where the fraction of four coordinated boron N_4 decreases with increasing fraction of Al_2O_3. The analysis of the ^{11}B NMR further shows that the proportion of B^{III} in non-ring configuration seems to remain constant, which indicates a reduction of the B^{IV}-O-Si linkage.

The Effect of Quenching on the Glass Structure

The effect of the thermal history on the network structure can be investigated comparing Raman spectra of a quenched and a furnace cooled sample (**Figure 4A**). The spectrum can be divided into four regions (see for comparison Möncke et al., 2015a). The small shift to higher values in the silicate network deformation mode (200–620 cm^{-1}) for the quenched sample can also be associated with a decrease of the inter-tetrahedral angle due to an increasing amount of smaller sized rings and/or an evolution of the Si-O-B connectivity. In the region between 700 and 850 cm^{-1} the typical modes for borate and boroxol rings can be observed. The borate peak loses intensity with increasing cooling rate (red arrow); a similar effect as observed by Al_2O_3 addition (blue arrow). The fraction of boroxol rings, in turn, behaves anti proportional to the effect of Al_2O_3 addition and decreases also with increasing cooling rate. In the region between 1,000 and 1,200 cm^{-1} which is associated with the bond stretching Si-O, Al-O, and B-O, a higher quenching rate has the same effect than the addition of Al with an increase of the contribution at 1,030 cm^{-1}. In the region between 1,250 and 1,600 cm^{-1} a slight decrease of the signal intensity around 1,500 cm^{-1} can be observed for the temperature treated sample. This decrease can be assigned to an increase of N_4 at higher cooling rate. Möncke et al. found the same trends in their investigations of the influence of the thermal history within this glass system. The increase of the mixed Si-O-B band at about 1,150 cm^{-1}, however, has not been observed in the present study (Möncke et al., 2015a). Those results show that a faster cooling rate results in a different glass network within or between the first coordination spheres. NMR supports those findings. All the recorded spectra (**Supplementary Figure 1**) are very similar. **Figures 4B,C** show the ^{11}B NMR and ^{27}Al NMR spectra of the 1.0 mol% Al quenched glass sample. From the ^{11}B spectra a change in the range of the B^{III} units can be observed. The proportion of B^{III} non-ring units is more pronounced compared to the B^{III} ring units. For the signal which can be assigned to the B^{IV} units a slight shift from 0.3 ppm to a higher chemical shift can be detected. This indicates a higher interconnectivity between the borate and silicate network in the quenched glasses. It is consistent with the results found in the Raman spectra and the literature (Möncke et al., 2006; Malchow et al., 2015). In the ^{27}Al NMR spectrum the linear shape remains constant and only a slight shift from 2 to 3 ppm to lower values is visible upon quenching. This means that the Al coordination is not affected by the cooling rate and that the bond Al-O is only slightly affected by the structural modifications mainly taking place in the vicinity of boron atoms. The proportion of B^{III} and B^{IV} is constant with increasing cooling rate, which is different from other borosilicate glasses (Angeli et al., 2012).

The Mechanical Properties

The mechanical properties of the NBS2 glass series are studied using nanoindentation and Brillouin spectroscopy. Brillouin spectroscopy allows to determine elastic material properties such as Young's modulus E, bulk modulus K, shear modulus G, P-wave

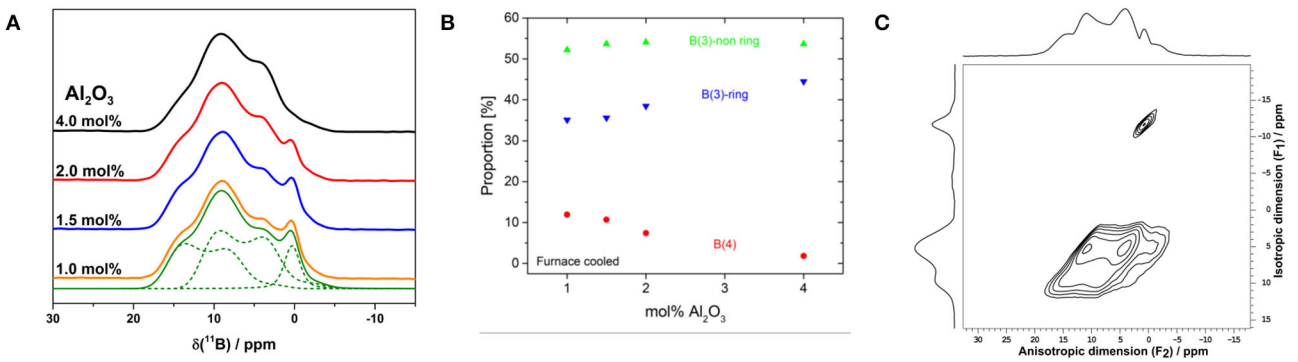

FIGURE 3 | (A) ^{11}B MAS-NMR at 500 MHz. The figure shows the evolution of three boron bands (two for three-fold coordinated and one for four-fold coordinated boron). Solid lines show the MAS spectra and the dotted lines show a typical deconvolution of ^{11}B NMR spectra using Multi Quantum MAS. The first dotted line with two peaks ranging from 18 to 5 ppm is assigned to B^{III} ring, the second line from 13 to 2 ppm to B^{III} non-ring and the third dotted line with a Gaussian shape centered at 0 ppm to B^{IV}. **(B)** The boron ring configuration according to ^{11}B-MAS NMR results for the furnace cooled glasses. **(C)** ^{11}B MQMAS-NMR-Spectra of the sample with 2.0 mol% Al_2O_3. Deconvolution of the three spectra in isolated signals.

TABLE 2 | The fraction of tetragonal boron: $N4_{NMR}$ are the results from NMR deconvolution.

NBS2 glass	$N4_{NMR}$	$R' = N_{4Charge\ compensation}$	$R = N_4$
1.0 mol% Al	0.12 ± 0.03	0.16 ± 0.02	0.21
1.5 mol% Al	0.11 ± 0.03	0.13 ± 0.02	0.21
2.0 mol% Al	0.07 ± 0.03	0.11 ± 0.02	0.21
4.0 mol% Al	0.02 ± 0.03	0.01 ± 0.02	0.21

For comparison the Dell and Bray model is applied for the nominal glass composition without the consideration of Al_2O_3 in that case, R gives the theoretical amount of B^{IV}. If Al_2O_3 is assumed to mobilize as charge compensator a fraction of the Na then a modified R factor called here R′ can be calculated (see text for more details).

modulus M, and Poisson's ratio ν if the density is known. For this purpose, density ρ was determined according to the principle of Archimedes. The determined parameters are summarized in **Table 3**. Both density and elastic properties slightly decrease with quenching rate. The addition of Al has no significant effect on density. The Poisson's ratio within the error bars remains constant for all the samples.

Nanoindentation testing probes the elastic-plastic material behavior and reveals that Young's modulus E values match the absolute values determined by Brillouin spectroscopy surprisingly well (**Table 3**). Moreover, the values obtained for the conventional NBS2 glass (containing 1 mol% Al_2O_3) agree well with the literature (Limbach et al., 2015). With an increased Al_2O_3 amount both hardness and modulus decrease (**Figure 5**). This tendency can be observed in furnace cooled as well as quenched glass. For a single glass composition an increasing cooling rate (quenching) results in lower H and E values, an observation supported by the literature (Ito and Taniguchi, 2004; Deng and Du, 2018). For the conventional NBS2 glass quenching interestingly has a similar effect on H and E as the addition of further 3.0 mol% Al_2O_3. This similitude is very interesting because it will allow us to analyze the structural modifications at iso elastic properties. Later on, in the discussion we will systematically compare these three key conditions: furnace cooled 1.0 mol% Al_2O_3, quenched 1.0 mol% Al_2O_3 and furnace cooled 4.0 mol% Al_2O_3.

The fracture behavior was studied with high load nanoindentation using various tip geometries. For Berkovich indentation the furnace cooled NBS2 glass (1 mol% Al_2O_3) shows mainly radial and conical cracking (**Figure 6A**). The crack systems occur mixed even for similar loading, so no clear trend could be observed.

Quenching the NBS2 glass (1.0 mol% Al_2O_3) to room temperature leads to a strongly stochastic cracking behavior and a significant increase in chipping and mixed fracture where many crack systems are active simultaneously (**Figure 6B**). Pure radial cracking does not appear at all while pure cone cracking can be observed to a very small amount.

The addition of Al_2O_3, in turn, unifies the crack pattern (**Figure 6C**). The 4.0 mol% Al_2O_3 containing NBS2 glass shows mainly edge cracks and lateral bright shining traces in the vicinity of the contact. When those cracks propagate to the surface they lead to chipping. Edge cracks are likely introduced by the tensile component, accompanied with sink-in upon loading, and typically penetrate only straight down to a very small depth (Mound and Pharr, 2019). Occasionally chipping can be observed, even at smaller loads.

Switching indenter geometries from the rather blunt Berkovich to the sharp cube corner tip unifies the cracking behavior within the NBS2 series. Radial cracking becomes predominant with increasing indenter sharpness, which is in good accordance with the literature (Gross, 2012; Bruns et al., 2020). However, cube corner indentation is usually accompanied with traces of chipping and, depending on the degree of chipping, the indentations show significant differences in radial crack extension (**Figure 6D**), ruling out a quantification of cracking according to Lawn et al. (1980).

The estimate of a fracture probability, however, allows to investigate qualitatively the cracking behavior of the borosilicate glass in terms of damage resistance value. In contrast to the

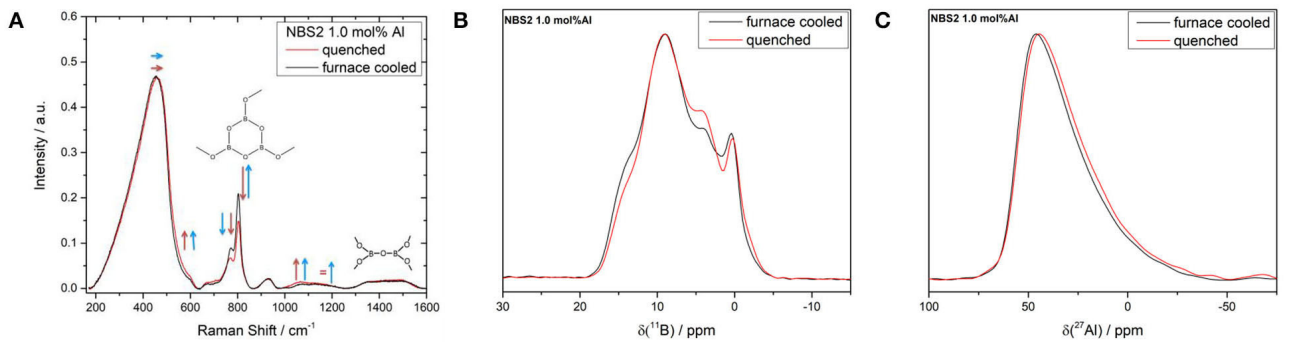

FIGURE 4 | (A) Thermal history effect on the glass structure obtained by Raman spectroscopy. Red arrows indicate changes by quenching while the blue arrows indicate changes upon Al_2O_3 addition for comparison. **(B)** ^{11}B-MAS NMR and **(C)** ^{27}Al-MAS NMR spectrum of a furnace cooled and quenched sample.

TABLE 3 | Density and mechanic properties of the investigated NBS2 glass series obtained by Brillouin spectroscopy and nanoindentation testing.

Al_2O_3 [mol%]	ρ [g/cm^3]	Brillouin shift Backscattering [GHz]	Brillouin shift Platelet transv./long. [GHz]	M [GPa]	ν	G [GPa]	K [GPa]	$E_{Brillouin}$ [GPa]	$E_{Indentation}$ [GPa]	H [GPa]
1.0	2.131 ± 0.006	30.62 ± 0.05	14.92 ± 0.02/8.86 ± 0.01	55.1 ± 0.4	0.228 ± 0.005	19.4 ± 0.4	29.2 ± 0.5	47.7 ± 0.7	47.6 ± 0.4	5.99 ± 0.04
1.0 qu.	2.122 ± 0.006	29.99 ± 0.05	14.43 ± 0.03/8.53 ± 0.03	52.9 ± 0.4	0.232 ± 0.005	18.4 ± 0.4	28.3 ± 0.5	45.4 ± 0.7	46.0 ± 0.2	5.64 ± 0.05
1.5	2.133 ± 0.010	30.60 ± 0.05	14,74 ± 0.01/8.73 ± 0.01	55.1 ± 0.6	0.230 ± 0.005	19.3 ± 0.5	29.4 ± 0.8	47.6 ± 1.2	47.5 ± 0.3	5.88 ± 0.04
1.5 qu.	2.132 ± 0.004	29.65 ± 0.05	14.52 ± 0.06/8.55 ± 0.03	51.9 ± 0.4	0.235 ± 0.005	18.0 ± 0.4	28.0 ± 0.5	44.5 ± 0.7	–	–
2.0	2.130 ± 0.002	30,41 ± 0.05	14.71 ± 0.03/8.69 ± 0.02	54.5 ± 0.3	0.232 ± 0.005	19.0 ± 0.4	29.1 ± 0.6	46.8 ± 0.8	46.1 ± 0.1	5.72 ± 0.04
2.0 qu.	2.124 ± 0.012	29,74 ± 0.05	14.41 ± 0.05/8.47 ± 0.03	52.0 ± 0.8	0.236 ± 0.005	18.0 ± 0.5	28.0 ± 0.7	44.4 ± 1.0	43.7 ± 0.2	5.32 ± 0.03
4.0	2.137 ± 0.004	30.35 ± 0.05	14.52 ± 0.04/8.59 ± 0.06	54.3 ± 0.2	0.235 ± 0.005	18.8 ± 0.3	29.2 ± 0.4	46.4 ± 0.6	45.5 ± 0.2	5.59 ± 0.02

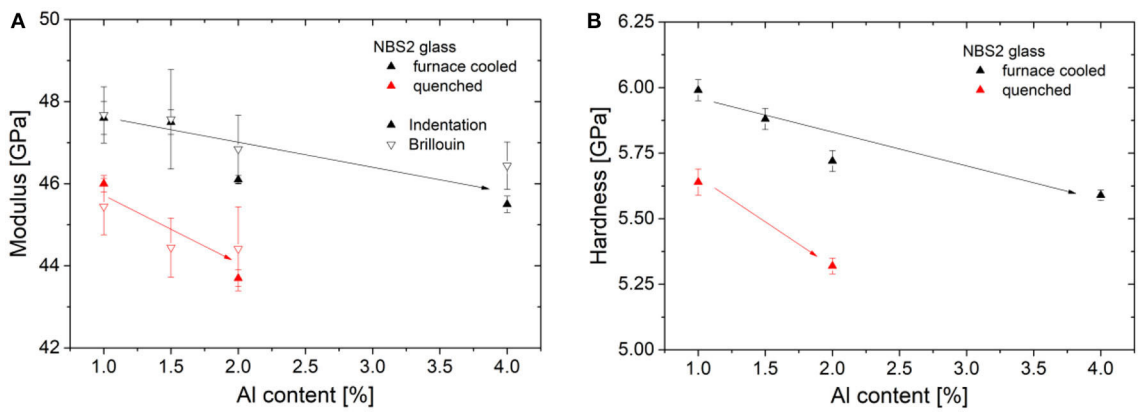

FIGURE 5 | (A) Young's modulus and **(B)** Hardness from nanoindentation testing (solid symbols). An estimate of Young's modulus from Brillouin spectroscopy is shown as open symbols. The thermal history, furnace cooled or quenched, is indicated by black or red color, respectively.

concept of Wada et al. (1974) and Kato et al. (2010), different crack systems are not differentiated in the present study. In this manner, the number of indents showing cracking N_{crack} was related to the total number of indentations N_{total} for a given indentation load.

Fracture probabilities were calculated for all examined indenter geometries, those for Vickers and cube corner tip geometry are shown in **Figure 7**, while Berkovich and 50° are provided as **Supplementary Data**. The rather blunt Berkovich or Vickers indenter exhibit huge scatter within the individual series, likely caused by the variety of the active crack system. The huge differences in crack morphology among the glasses complicates a further comparison. However, using the sharper cube-corner indenter, with a decreasing indenter centerline-to-face angle, the fracture probability is better defined and the scatter decreases. The profiles can be fitted with a sigmoidal function

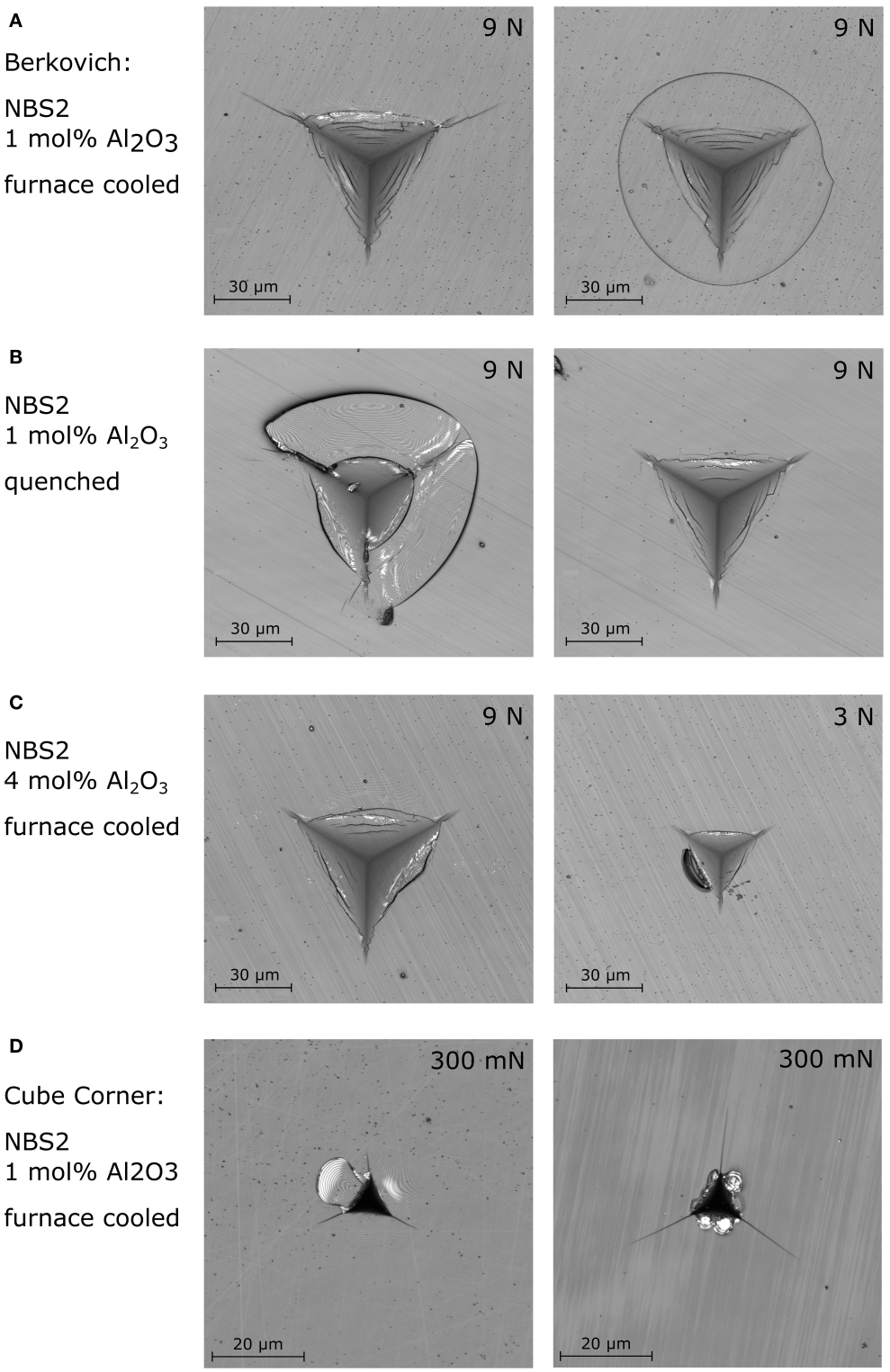

FIGURE 6 | Indentation cracking upon Berkovich indentation in **(A)** furnace cooled and **(B)** quenched NBS2 glass containing 1 mol% Al_2O_3 as well as **(C)** in furnace cooled NBS2 with a larger Al_2O_3 content of 4 mol%. **(D)** Cube corner indentation cracking in conventional furnace cooled NBS2 glass. Even though the loading is equal in both cases, the radial crack length scatters from 11.8 ± 0.8 µm (left) to 21.4 ± 0.4 µm (right), depending on the extent of chipping.

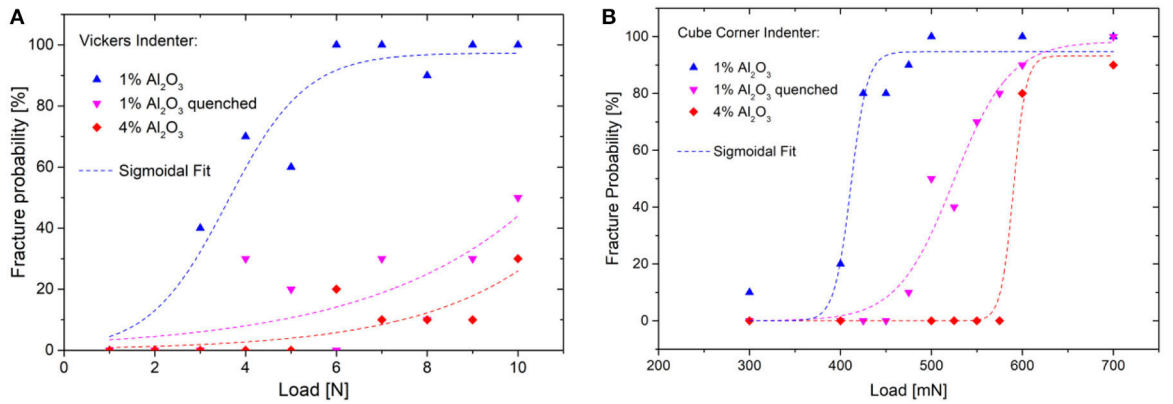

FIGURE 7 | Fracture probability of the NBS2 glass series for **(A)** Vickers and **(B)** Cube Corner nanoindentation.

TABLE 4 | Fracture initiation load in N, determined with sigmoidal fits from fracture probability plots (**Figure 7**).

NBS2 glass	Fracture initiation load [*N*]		
	Vickers (4-sided)	50° (3-sided)	Cube corner (3-sided)
1.0 mol% Al	3.65	0.62	0.41
1.0 mol% Al, quenched	≈10.0	3.27	0.53
4.0 mol% Al	>10.0	3.27	0.59

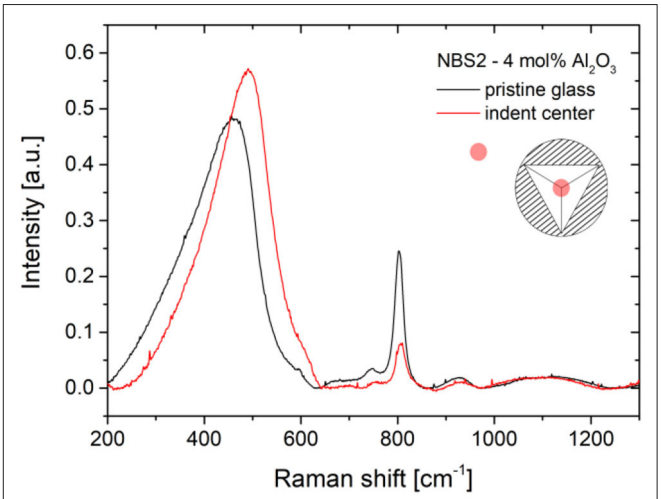

FIGURE 8 | Changes in the area normalized Raman spectra induced by indentation in furnace cooled NBS2 glass (4 mol% Al_2O_3). The black curve represents the pristine condition while the red curve is measured at indent center.

to determine a fracture initiation load, which is here defined as the corresponding load for 50% fracture probability. For the Berkovich geometry, scatter was too high to allow a sigmoidal fit, hence this tip geometry is not listed in **Table 4**.

For all examined indenter geometries, the furnace cooled NBS2 glass containing 1.0 mol% Al_2O_3 exhibits the lowest cracking threshold value. Quenching shifts the threshold values toward higher loads as reported in the literature (Malchow et al., 2015). In a similar manner the fracture initiation loads shifts, with the addition of Al_2O_3 further. Especially for sharper tip geometries, the 4.0 mol% Al_2O_3 containing NBS2 glass exhibits even slightly larger threshold values as samples prepared under the quenched condition.

In the literature, enhanced fracture properties of the quenched state were attributed to an increased interconnectivity between the borate and silicate subnetworks (shown by a small negative shift of 0.3 ppm of the B^{IV} unit from furnace cooled to quenched glass), but also to the smaller packing density and the accompanied larger densification ability provided by the glass prepared under quenching conditions (Malchow et al., 2015). To further elucidate these effects, the glass structure of the three key conditions is analyzed by Raman spectroscopy, comparing spectra at indent center to those of pristine glass (**Figure 8**).

Deformation is accompanied with a significant shift and intensity increase of the deformation band below 600 cm^{-1}, which is called main band in pure SiO_2 glass (**Figure 8**). The boroxol and borate ring breathing bands, in turn, decrease in intensity. This tendency was observed for all three key conditions (1.0 mol% Al_2O_3 furnace cooled and quenched, as well as 4.0 mol% Al_2O_3 furnace cooled). The comparison of the remaining spectra is provided as **Supplementary Data**. The deformation band shift is analyzed according to the procedure proposed by Deschamps et al. (2011, 2013) by defining a half integral main band centroid σ as a measure for the main band position. They established a linear relationship between the band shift Δσ and densification $\Delta\rho/\rho_0$ according to:

$$\frac{\Delta p}{p}\,[\%] = m \times \Delta\sigma \tag{2}$$

To the best of the author's knowledge a correlation factor m for borosilicate glasses has not been determined yet. Deschamps et al.

TABLE 5 | Raman study of the deformation process present during indentation.

NBS2 glass	$\sigma_{pristine}$ [cm^{-1}]	σ_{center} [cm^{-1}]	$\Delta\sigma$ [cm^{-1}]	Densification [%]*
1.0 mol% Al	424	467	43	8.6
1.0 mol% Al qu.	430	470	40	8
4.0 mol% Al	430	469	39	7.8

*Raman spectroscopy was performed in indent center and for comparison in the unaffected base material. *Densification is determined using a correlation factor for SiO_2, which may not be applicable to borosilicate glasses.*

(2011, 2013) established a correlation factor m = 0.2% cm for pure SiO_2 which was used in this study instead. The densification deduced and shown in **Table 5** is then only given an order of magnitude but reflects well the trend between the differences.

All glasses exhibit comparable σ values at the center of the indent. A small difference can be observed for the pristine glass. Here the conventional NBS2 glass is located at 424 cm^{-1}, while the quenched and the 4.0 mol% Al_2O_3 containing glass are located at 430 cm^{-1}. This offset corresponds to the shift of the deformation band found in **Figures 1B**, **4**, and the variation of intensity of the D2 band causing a little larger $\Delta\sigma$.

DISCUSSION

With increasing the content of Al_2O_3 within the sodium borosilicate glass, the boroxol amount increases at the cost of B^{IV} units. This tendency can be observed with both spectroscopical methods used in the present study, Raman (**Figure 1**) and NMR (**Figure 3**) spectroscopy. Most likely Al is inserted into a former B^{IV}-O-Si bridge. Thereby B^{IV} is transformed into a B^{III} unit and Aluminum takes the role as network former, linking Si and B subnetworks. The ^{27}Al MAS-NMR spectra further indicate that the structure within the present glasses is dominated by a four-fold coordination of Al, described as $[AlO_4]^-$ units, which is charge compensated by Na^+ (**Figure 9**). The tendency of boron to form a four-fold coordination depends strongly on the glass composition (Dell et al., 1983), i.e., the type and availability of network modifier species (Kim and Bray, 1974; Angeli et al., 2010), and in the given sodium borosilicate glass, B^{IV} seems to form only with the modifier cations remaining after Al-modification. This behavior is in good accordance with the literature as it has also been observed in other alumino borosilicate glasses (Osipov et al., 2016; Frederiksen et al., 2018; Bradtmüller et al., 2019). As Al is preferred for charge compensation of the Na^+ species, the formation of $[AlO_4]^-$ units indirectly influences the boron modification, which is then limited by the remaining fraction of Na^+. In our modification of the Dell and Bray model (Equation 1) the concentration of B^{IV} units is predicted by taking this behavior into consideration. The experimental N_4-NMR values are only slightly lower than those delivered by our prediction (Equation 1), which might be ascribed to some loss of sodium ions during melting.

Based on those results a structural model for the incorporation of Al_2O_3 in the structure of the sodium borosilicate glass NBS2 can be developed (**Figure 9**).

With regard to the mechanical properties, those structural changes were found to go hand in hand with a softening, as seen in a reduction of the elastic modulus and hardness. Both effects can be attributed to the increasing amount of more flexible trigonal borate units, which softens the network due to its planar nature, leading to a larger free volume for B^{III} and a subsequently reduced stiffness of the glass network (Eagan and Swearekgen, 1978; Inaba et al., 1999; Januchta et al., 2019b). Moreover, both quenching and the alumina addition shifts the fracture initiation load toward higher values for all examined tip geometries (**Figure 7**). An investigation of deformation-induced Raman band shifts upon indentation was performed on the two extreme cases in order to elucidate whether the enhanced fracture initiation behavior can be attributed to significant changes in the predominant deformation process. The study, however, reveals $\Delta\sigma$ values in a similar range, so no significant change in densification ability of the glasses occurred. Hence, the enhanced crack resistance of the 4 mol% Al_2O_3 glass cannot be attributed to densification. This observation is in agreement with a recent study on alumino borosilicate glasses by Januchta et al. (2019a), who neither found a direct correlation between the fracture initiation resistance and densification. The significant changes in the fraction of boroxol and borate rings upon indentation rather indicate that those units have played a significant role during deformation. The Raman study on the pristine glasses has shown that glasses with larger Al_2O_3 content exhibit a larger share of planar B^{III} units (**Figure 1**). It is well-known in the literature that the reduced three dimensionality of the boron network favors shear deformation (Yoshida et al., 2009; Januchta and Smedskjaer, 2019). In a similar manner the intensity of the band related to planar B^{III} rings (750–800 cm^{-1}) is greatly reduced during indentation (**Figure 8**). Glasses with high Al_2O_3 content exhibit more planar boroxol units, hence, a shear softening effect becomes visible, which manifests in a reduced glass hardness (**Figure 5**), similar as found in comparable glass systems in literature (Januchta et al., 2019a,b). Januchta et al. (2019b) discusses a correlation between cracking and the boron configuration. While the crack front has to break B-O bonds if boron is arranged in rigid tetrahedra, bond breakage might be avoided if trigonal boron arranges in planar rings. It can be imagined that adjacent borate rings can be separated without the need of breaking any bond. Thus, the enhanced fracture initiation properties of NBS2 glasses with high Al_2O_3 are likely to be attributed to the larger share of trigonal boron present in those glasses. For the quenched glasses the Raman study at indent center exhibits a strong intensity decrease of the band related to planar B^{III} rings (750–800 cm^{-1}). This indicates that those structural units are involved in deformation. Moreover, the band related to B^{IV} units (∼770 and 760 cm^{-1}) is more intense in this qu 1 mol% Al_2O_3 glass compared to the fc 4 mol% Al_2O_3 configuration. A significant intensity decrease of this B^{IV} band upon deformation can be observed there, too. Unfortunately, the given dataset does not allow for a final conclusion. It is, however, natural that the structural change induced by quenching is different from that induced by an addition of Al_2O_3. It is therefore normal that the deformation of these glasses is different to a certain extent even though E, H, and the fracture initiation properties point in a similar direction.

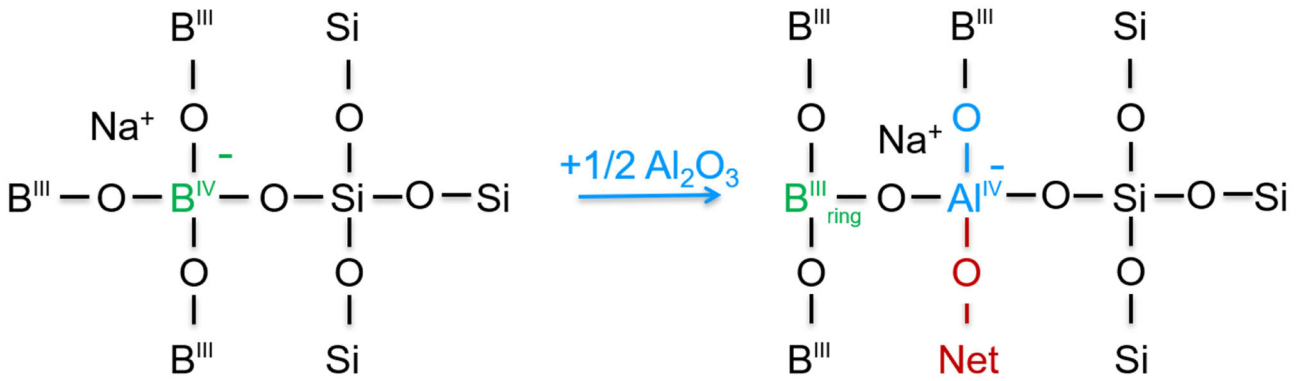

FIGURE 9 | Structural change upon ½ Al_2O_3 addition in the NBS2 sodium borosilicate glass. The ½ O is shared with the network Net represented in red. The B^{IV} changed to a B^{III}_{ring} represented in green here.

Even if elucidating the exact superstructural units connecting aluminate, borate and silicate is a very difficult task and remains therefore speculative, some improvement of the global connectivity can be observed in both quench and Al enriched samples. In the earlier studies on the influence of the annealing rate on the mechanical properties of NBS2, the intermediate range order and connectivity between borate and silicate units were given much focus. Quenching improved the interconnectivity of borate and silicate units in this low alkali borosilicate glass. Indeed, it was shown that trigonal borate had a higher tendency to bond to silicate than tetrahedral borate. Differently, alumina is known to reduce the tendency of phase separation. Its addition helps to close the immiscibility gap, increases the fraction of trigonal borate and therefore increases overall the interconnectivity between network formers. Hence, if it is too complex to attribute the enhanced fracture initiation properties to certain structural units, the interconnectivity between network formers seems to play a central role in both cases.

Finally, it is worth noting that an enhanced fracture initiation load does not correspond to a higher fracture toughness, which describes the critical stress intensity factor for crack growth (Rouxel and Yoshida, 2017; Januchta et al., 2019a). Concerning the fracture toughness, it is even disadvantageous if the crack can surpass certain structural units (e.g., boroxol rings) and has to break less bonds on its way through the material (Januchta et al., 2019b). As the fracture toughness is directly linked to bond strength and packing density, similar to the elastic modulus, it is expected to correlate with E (Rouxel, 2017; Januchta et al., 2019a). In this manner the decrease in the elastic modulus indicates a fracture toughness reduction for the NBS2 glass with higher alumina content and after quenching.

CONCLUSION

The addition of Al_2O_3 is a promising approach for improving the crack initiation loading NBS2 sodium borosilicate glass and, hence, for replicating the effect quenching has on the mechanical properties in this system. In general, both approaches of Al_2O_3 addition and quenching aim to prevent phase separation of the boron and silica subnetworks. Increasing the Al_2O_3 content from 1.0 to 4.0 mol% results in more Al-ions acting as network former linking Si to B units, while four-fold coordination ensures charge compensation sites for Na^+. It is obvious that quenching increases the network interconnectivity differently, since the share of Al_2O_3 is constant. Even though quenching and Al-additions lead to the formation of different network structures within the glass, the effect on the mechanical response is comparable and both the modified NBS2 glass with the highest Al_2O_3 content of 4.0 mol% and the quenched state of the conventional NBS2 glass (1.0 mol% Al_2O_3) exhibit remarkably similar modulus and hardness values. The fracture initiation load shifts toward higher loads following both approaches. The different network structures forming upon Al_2O_3 addition and quenching, however, manifest in differences in the crack pattern. While under the quenched condition a variety of crack systems is activated due to local variations in the glass structure, the addition of Al_2O_3 unifies the crack pattern and reduces scatter in the fracture probability plots (**Figure 7**). In this manner, Al_2O_3 represents a more reliable approach for improving the fracture initiation behavior of borosilicate glass.

While in the literature the improvement of fracture properties is often attributed to a more pronounced densification ability of the enhanced glass (Malchow et al., 2015), recent studies question whether densification alone can enable such significant improvements (Bruns et al., 2017). Raman investigations along indents reveal comparable band shifts for all examined glasses within the present study. Those results clearly show that the gain in fracture initiation cannot be attributed to densification effects alone. The decrease in hardness rather indicates a shear softening accompanied with a smaller driven force for crack initiation in the glasses with improved fracture behavior.

DATA AVAILABILITY STATEMENT

All datasets generated for this study are included in the article/**Supplementary Material**.

AUTHOR CONTRIBUTIONS

DM, DL, and KD developed the basic idea for the presented project. TU produced the glasses and carried out and evaluated the spectroscopic investigations. SB and DW carried out and evaluated mechanical measurements, the theoretical simulations, evaluation and analysis of the data, and contributed ideas. DM, DL, KD, and LW supported TU. All authors worked together in interpreting and linking the measurement results. All authors have discussed the results and collaborated on the manuscript.

FUNDING

Financial support from the German Science Foundation DFG through the priority program 1594 Topological Engineering of Ultra-Strong Glasses (DU 424/8-2 and MO 1375/3-2) was gratefully acknowledged.

SUPPLEMENTARY MATERIAL

The Supplementary Material for this article can be found online at: https://www.frontiersin.org/articles/10.3389/fmats.2020.00189/full#supplementary-material

REFERENCES

Angeli, F., Charpentier, T., De Ligny, D., and Cailleteau, C. (2010). Boron speciation in soda-lime borosilicate glasses containing zirconium. *J. Am. Ceram. Soc.* 93, 2693–2704. doi: 10.1111/j.1551-2916.2010.03771.x

Angeli, F., Villain, O., Schuller, S., Charpentier, T., de Ligny, D., Bressel, L., et al. (2012). Effect of temperature and thermal history on borosilicate glass structure. *Phys. Rev. B* 85:054110. doi: 10.1103/PhysRevB.85.054110

Barlet, M., Delaye, J.-M., Charpentier, T., Gennisson, M., Bonamy, D., Rouxel, T., et al. (2015). Hardness and toughness of sodium borosilicate glasses via Vickers's indentations. *J. Non Cryst. Solids* 417–418, 66–79. doi: 10.1016/j.jnoncrysol.2015.02.005

Biscoe, J., and Warren, B. E. (1938). X-ray diffraction study of soda-boric oxide glass. *J. Am. Ceram. Soc.* 21, 287–293. doi: 10.1111/j.1151-2916.1938.tb15777.x

Bradtmüller, H., Uesbeck, T., Eckert, H., Murata, T., Nakane, S., and Yamazaki, H. (2019). Structural origins of crack resistance on magnesium aluminoborosilicate glasses studied by solid-state NMR. *J. Phys. Chem. C* 123, 14941–14954. doi: 10.1021/acs.jpcc.9b03600

Bruns, S., Johanns, K. E., Rehman, H. U. R., Pharr, G. M., and Durst, K. (2017). Constitutive modeling of indentation cracking in fused silica. *J. Am. Ceram. Soc.* 100, 1928–1940. doi: 10.1111/jace.14734

Bruns, S., Petho, L., Minnert, C., Michler, J., and Durst, K. (2020). Fracture toughness determination of fused silica by cube corner indentation cracking and pillar splitting. *Mater. Design* 186:108311. doi: 10.1016/j.matdes.2019.108311

Dell, W. J., Bray, P. J., Xiao, S. Z. (1983). 11B NMR studies and structural modeling of Na_2O-B_2O_3-SiO_2 glasses of high soda content. *J. Non Cryst. Solids* 58, 1–16. doi: 10.1016/0022-3093(83)90097-2

Deng, L., and Du, J. (2018). Effects of system size and cooling rate on the structure and properties of sodium borosilicate glasses from molecular dynamics simulations. *J. Chem. Phys.* 148:024504. doi: 10.1063/1.5007083

Deschamps, T., Kassir-Bodon, A., Sonneville, C., Margueritat, J., Martinet, C., de Ligny, D., et al. (2013). Permanent densification of compressed silica glass: a Raman-density calibration curve. *J. Phys. Condens Matter.* 25:025402. doi: 10.1088/0953-8984/25/2/025402

Deschamps, T., Martinet, C., Bruneel, J. L., and Champagnon, B. (2011). Soda-lime silicate glass under hydrostatic pressure and indentation: a micro-Raman study. *J. Phys. Condens. Matter.* 23:035402. doi: 10.1088/0953-8984/23/3/035402

Du, L.-S., and Stebbins, J. F. (2003). Solid-state NMR study of metastable immiscibility in alkali borosilicate glasses. *J. Non Cryst. Solids* 315, 239–255. doi: 10.1016/S0022-3093(02)01604-6

Eagan, R. J., and Swearekgen, J. (1978). Effect of composition on the mechanical properties of aluminosilicate and borosilicate glasses. *J. Am. Ceram. Soc.* 61, 27–30. doi: 10.1111/j.1151-2916.1978.tb09222.x

Eckert, H. (1992). Structural characterization of noncrystalline solids and glasses using solid state NMR. *Prog. Nucl. Magn. Reson Spectrosc.* 24, 159–293. doi: 10.1016/0079-6565(92)80001-V

Eckert, H. (1994). "Structural studies of noncrystalline solids using solid state NMR.: new experimental approaches and results," in *Solid-State NMR IV Methods and Applications of Solid-State NMR* (Berlin; Heidelberg: Springer), 125–98. doi: 10.1007/978-3-642-79127-7_3

Eden, M. (2015). "^{27}Al NMR studies of aluminosilicate glasses," in *Annual Reports on NMR Spectroscopy*, *Vol. 86* (Waltham, MA; San Diego, CA; London; Oxford: Elsevier), 237–331. doi: 10.1016/bs.arnmr.2015.04.004

Ehrt, D. (2000). Structure, properties and applications of borate glasses. *Glass Technol.* 41, 182–185.

Ellison, A., and Cornejo, I. A. (2010). Glass substrates for liquid crystal displays. *Int. J. Appl. Glass Sci.* 1, 87–103. doi: 10.1111/j.2041-1294.2010.00009.x

Frederiksen, K. F., Januchta, K., Mascaraque, N., Youngman, R. E., Bauchy, M., Rzoska, S. J., et al. (2018). Structural compromise between high hardness and crack resistance in aluminoborate glasses. *J. Phys. Chem. B* 122, 6287–6295. doi: 10.1021/acs.jpcb.8b02905

Gross, T. M. (2012). Deformation and cracking behavior of glasses indented with diamond tips of various sharpness. *J. Non Cryst. Solids* 358, 3445–3452. doi: 10.1016/j.jnoncrysol.2012.01.052

Gross, T. M., and Price, J. J. (2017). Vickers indentation cracking of ion-exchanged glasses: Quasi-static vs. dynamic contact. *Front. Mater.* 4, 1–14. doi: 10.3389/fmats.2017.00004

Inaba, S., Fujino, S., and Morinaga, K. (1999). Young's modulus and compositional parameters of oxide glasses. *J. Am. Ceram. Soc.* 82, 3501–3507. doi: 10.1111/j.1151-2916.1999.tb02272.x

Ito, S., and Taniguchi, T. (2004). Effect of cooling rate on structure and mechanical behavior of glass by MD simulation. *J. Non Cryst. Solids* 349, 173–179. doi: 10.1016/j.jnoncrysol.2004.08.180

Januchta, K., Liu, P., Hansen, S. R., To, T., and Smedskjaer, M. M. (2019a). Indentation cracking and deformation mechanism of sodium aluminoborosilicate glasses. *J. Am. Ceram. Soc.* 103, 1656–1665. doi: 10.1111/jace.16894

Januchta, K., and Smedskjaer, M. M. (2019). Indentation deformation in oxide glasses: quantification, structural changes, and relation to cracking. *J. Non Cryst. Solids X* 1:100007. doi: 10.1016/j.nocx.2018.100007

Januchta, K., To, T., Bødker, M. S., Rouxel, T., and Smedskjaer, M. M. (2019b). Elasticity, hardness, and fracture toughness of sodium aluminoborosilicate glasses. *J. Am. Ceram. Soc.* 102, 4520–4537. doi: 10.1111/jace.16304

Januchta, K., Youngman, R. E., Goel, A., Bauchy, M., Logunov, S. L., Rzoska, S. J., et al. (2017). Discovery of ultra-crack-resistant oxide glasses with adaptive networks. *Chem. Mater.* 29, 5865–5876. doi: 10.1021/acs.chemmater.7b00921

Kato, Y., Yamazaki, H., Yoshida, S., and Matsuoka, J. (2010). Effect of densification on crack initiation under Vickers indentation test. *J. Non Cryst. Solids* 356, 1768–1773. doi: 10.1016/j.jnoncrysol.2010.07.015

Kim, K. S., and Bray, P. J. (1974). B^{11} NMR studies of glasses in the system MgO-Na_2O-B_2O_3. *Phys. Chem. Glasses* 15, 47–51.

Kurkjian, C. R., Gupta, P. K., and Brow, R. K. (2010). The strength of silicate glasses: what do we know, what do we need to know? *Int. J. Appl. Glass Sci.* 1, 27–37. doi: 10.1111/j.2041-1294.2010.00005.x

Lawn, B. R., Evans, A. G., and Marshall, D. B. (1980). Elastic-plastic indentation damage in ceramics - the median-radial crack system. *J. Am. Ceram. Soc.* 63, 574–581. doi: 10.1111/j.1151-2916.1980.tb10768.x

Limbach, R., Winterstein-Beckmann, A., Dellith, J., Möncke, D., and Wondraczek, L. (2015). Plasticity, crack initiation and defect resistance in alkali-borosilicate glasses: from normal to anomalous behavior. *J. Non Cryst. Solids* 417–418, 15–27. doi: 10.1016/j.jnoncrysol.2015.02.019

MacKenzie, K. J., and Smith, M. E. (2002). *Multinuclear Solid-State Nuclear Magnetic Resonance of Inorganic Materials*. Oxford: Elsevier.

Malchow, P., Johanns, K. E., Möncke, D., Korte-Kerzel, S., Wondraczek, L., and Durst, K. (2015). Composition and cooling-rate dependence of plastic deformation, densification, and cracking in sodium borosilicate

glasses during pyramidal indentation. *J. Non Cryst. Solids* 419, 97–109. doi: 10.1016/j.jnoncrysol.2015.03.020

Martens, R., and Müller-Warmuth, W. (2000). Structural groups and their mixing in borosilicate glasses of various compositions – an NMR study. *J. Non Cryst. Solids* 265, 167–175. doi: 10.1016/S0022-3093(99)00693-6

Massiot, D., Fayon, F., Capron, M., King, I., Le Calvé, S., Alonso, B., et al. (2002). Modelling one- and two-dimensional solid-state NMR spectra. *Magn. Reson. Chem.* 40, 70–76. doi: 10.1002/mrc.984

Mauro, J. C. (2014). Grand challenges in glass science. *Front. Mater.* 1:20. doi: 10.3389/fmats.2014.00020

Medek, A., Harwood, J. S., and Frydman, L. (1995). Multiple-quantum magic-angle spinning NMR: a new method for the study of quadrupolar nuclei in solids. *J. Am. Chem. Soc.* 117, 12779–12787. doi: 10.1021/ja00156a015

Milberg, M. E., O'Keefe, J. G., Verhelst, R. A., and Hooper, H. O. (1972). Boron coordination in sodium borosilicate glasses. *Phys. Chem. Glasses* 13, 79–84.

Möncke, D., Ehrt, D., Eckert, H., and Mertens, V. (2003). Influence of melting and annealing conditions on the structure of borosilicate glasses. *Phys. Chem. Glasses* 44, 113–116.

Möncke, D., Ehrt, D., Tricot, G., and Kamitsos, E. I. (2015a). Connectivity of borate and silicate groups in a low-alkali borosilicate glass by vibrational and 2D NMR spectroscopy. *J. Chem. Technol. Metallurgy* 50, 381–386.

Möncke, D., Ehrt, D., Varsamis, C. P. E., Kamitsos, E. I., and Kalampounias, A. G. (2006). Thermal history of a low alkali borosilicate glass probed by infrared and Raman spectroscopy. *Glass Technol. Eur. J. Glass Sci. Technol. A* 47, 133–137.

Möncke, D., Tricot, G., Winterstein-Beckmann, A., Wondraczek, L., and Kamitsos, E. I. (2015b). On the connectivity of borate tetrahedra in borate and borosilicate glasses. *Phys. Chem. Glasses Eur. J. Glass Sci. Technol. B* 56, 203–211. doi: 10.13036/1753-3562.56.5.203

Mound, B. A., and Pharr, G. M. (2019). Nanoindentation of fused quartz at loads near the cracking threshold. *Exp. Mech.* 59, 369–380. doi: 10.1007/s11340-018-00446-3

Oliver, W. C., and Pharr, G. M. (1992). An improved technique for determining hardness and elastic-modulus using load and displacement sensing indentation experiments. *J. Mater. Res.* 7, 1564–1583. doi: 10.1557/JMR.1992.1564

Osipov, A. A., Eremyashev, V. E., Mazur, A. S., Tolstoi, P. M., and Osipova, L. M. (2016). Coordination state of aluminum and boron in barium aluminoborate glass. *Glass Phys. Chem.* 42, 230–237. doi: 10.1134/S1087659616030111

Polian, A. (2003). Brillouin scattering at high pressure: an overview. *J. Raman Spectrosc.* 34, 633–637. doi: 10.1002/jrs.1031

Price, J. J., Glaesemann, G. S., Clark, D. A., Gross, T. M., and Barefoot, K. L. (2009). "69.3: a mechanics framework for ion-exchanged cover glass with a deep compression layer," in *SID Symposium Digest of Technical Papers*, *Vol. 40*, 1049–1051. doi: 10.1889/1.3256467

Reibstein, S., Wondraczek, L., de Ligny, D., Krolikowski, S., Sirotkin, S., Simon, J. P., et al. (2011). Structural heterogeneity and pressure-relaxation in compressed borosilicate glasses by in situ small angle X-ray scattering. *J. Chem. Phys.* 134:204502. doi: 10.1063/1.3593399

Rosales-Sosa, G. A., Masuno, A., Higo, Y., and Inoue, H. (2016). Crack-resistant Al_2O_3-SiO_2 glasses. *Sci. Rep.* 6:23620. doi: 10.1038/srep23620

Rouxel, T. (2007). Elastic properties and short-to medium-range order in glasses. *J. Am. Ceram. Soc.* 90, 3019–3039. doi: 10.1111/j.1551-2916.2007.01945.x

Rouxel, T. (2015). Driving force for indentation cracking in glass: composition, pressure and temperature dependence. *Philos. Trans. A Math. Phys. Eng. Sci.* 373, 1–26. doi: 10.1098/rsta.2014.0140

Rouxel, T. (2017). Fracture surface energy and toughness of inorganic glasses. *Scr. Mater.* 137, 109–113. doi: 10.1016/j.scriptamat.2017.05.005

Rouxel, T., and Yoshida, S. (2017). The fracture toughness of inorganic glasses. *J. Am. Ceram. Soc.* 100, 4374–4396. doi: 10.1111/jace.15108

Smedskjaer, M. M., Youngman, R. E., and Mauro, J. C. (2014). Principles of Pyrex® glass chemistry: structure–property relationships. *Appl. Phys. A* 116, 491–504. doi: 10.1007/s00339-014-8396-1

Stebbins, J. F., Zhao, P., and Kroeker, S. (2000). Non-bridging oxygens in borate glasses: characterization by ^{11}B and ^{17}O MAS and 3QMAS NMR. *Solid State Nuclear Magnet. Reson.* 16, 9–19. doi: 10.1016/S0926-2040(00)00050-3

van Wüllen, L., and Schwering, G. (2002). ^{11}B-MQMAS and ^{29}Si-^{11}B double-Resonance NMR studies on the structure of binary B_2O_3-SiO_2 glasses. *Solid State Nucl. Magn. Reson.* 21, 134–144. doi: 10.1006/snmr.2002.0054

Veber, A., Cicconi, M. R., Reinfelder, H., and De Ligny, D. (2017). Combined differential scanning calorimetry, Raman and Brillouin spectroscopies: a multiscale approach for materials investigation. *Analyt. Chim. Acta* 998:37–44. doi: 10.1016/j.aca.2017.09.045

Vogel, W. (1994). *Glass Chemistry, 2nd edn,* Vol. 14. Berlin; Heidelberg: Springer, 464. doi: 10.1007/978-3-642-78723-2

Wada, M., Furukawa, H., and Fujita, K. (eds.). (1974). Crack resistance of glass on Vickers indentation. *Proc. Int. Congr. Glass* 11, 39–46.

Wang, S., and Stebbins, J. F. (1998). On the structure of borosilicate glasses: a triple-quantum magic-angle spinning ^{17}O nuclear magnetic resonance study. *J. Non Cryst. Solids* 231, 286–290. doi: 10.1016/S0022-3093(98)00703-0

Winterstein-Beckmann, A., Möncke, D., Palles, D., Kamitsos, E. I., and Wondraczek, L. (2013). Structure–property correlations in highly modified Sr, Mn-borate glasses. *J. Non Cryst Solids* 376, 165–174. doi: 10.1016/j.jnoncrysol.2013.05.029

Winterstein-Beckmann, A., Möncke, D., Palles, D., Kamitsos, E. I., and Wondraczek, L. (2014a). Raman spectroscopic study of structural changes induced by micro-indentation in low alkali borosilicate glasses. *J. Non Cryst. Solids* 401, 110–114. doi: 10.1016/j.jnoncrysol.2013.12.038

Winterstein-Beckmann, A., Möncke, D., Palles, D., Kamitsos, E. I., and Wondraczek, L. (2014b). A Raman-spectroscopic study of indentation-induced structural changes in technical alkali-borosilicate glasses with varying silicate network connectivity. *J. Non Cryst. Solids* 405, 196–206. doi: 10.1016/j.jnoncrysol.2014.09.020

Wondraczek, L., Krolikowski, S., and Behrens, H. (2010). Kinetics of pressure relaxation in a compressed alkali borosilicate glass. *J. Non Cryst. Solids* 356, 1859–1862. doi: 10.1016/j.jnoncrysol.2010.06.009

Wondraczek, L., Mauro, J. C., Eckert, J., Kühn, U., Horbach, J., Deubener, J., et al. (2011). Towards ultrastrong glasses. *Adv. Mater.* 23, 4578–4586. doi: 10.1002/adma.201102795

Wondraczek, L., Sen, S., Behrens, H., and Youngman, R. E. (2007). Structure-energy map of alkali borosilicate glasses: effects of pressure and temperature. *Phys. Rev. B* 76:014202. doi: 10.1103/PhysRevB.76.014202

Yoshida, S. (2019). Indentation deformation and cracking in oxide glass – toward understanding of crack nucleation. *J. Non Cryst. Solids X* 1:100009. doi: 10.1016/j.nocx.2019.100009

Yoshida, S., Hayashi, Y., Konno, A., Sugawara, T., Miura, Y., and Matsuoka, J. (2009). Indentation induced densification of sodium borate glasses. *Phys. Chem. Glass.* 50, 63–70.

Yoshida, S., Wada, K., Fujimura, T., Yamada, A., Kato, M., Matsuoka, J., et al. (2016). Evaluation of sinking-in and cracking behavior of soda-lime glass under varying angle of trigonal pyramid indenter. *Front. Mater.* 3:54. doi: 10.3389/fmats.2016.00054

Yun, Y., and Bray, P. (1978). Nuclear magnetic resonance studies of the glasses in the system Na_2O-B_2O_3-SiO_2. *J. Non Cryst. Solids* 27, 363–380. doi: 10.1016/0022-3093(78)90020-0

Yun, Y. H., Feller, S. A., and Bray, P. J. (1979). Correction and addendum to Nuclear Magnetic-Resonance studies of the glasses in the system Na_2O-B_2O_3-SiO_2. *J. Non Cryst. Solids* 33, 273–277. doi: 10.1016/0022-3093(79)90055-3

Zehnder, C., Bruns, S., Peltzer, J. N., Durst, K., Korte-Kerzel, S., and Möncke, D. (2017a). Influence of cooling rate on cracking and plastic deformation during impact and indentation of borosilicate glasses. *Front. Mater.* 4:5. doi: 10.3389/fmats.2017.00005

Zehnder, C., Peltzer, J.-N., Gibson, J. S. K. L., Möncke, D., and Korte-Kerzel, S. (2017b). Non-Newtonian flow to the theoretical strength of glasses via impact nanoindentation at room temperature. *Sci. Rep.* 7:17618. doi: 10.1038/s41598-017-17871-4

Conflict of Interest: The authors declare that the research was conducted in the absence of any commercial or financial relationships that could be construed as a potential conflict of interest.